Investigation of large enhancement of spin hall angle in heterostructures of Ag nanoparticles randomly grown in Pt

Cite as: AIP Advances **9**, 035025 (2019); https://doi.org/10.1063/1.5079813
Submitted: 03 November 2018 . Accepted: 17 January 2019 . Published Online: 15 March 2019

O. Alves Santos, E. F. Silva, M. Gamino, J. B. S. Mendes, S. M. Rezende, and A. Azevedo

Investigation of large enhancement of spin hall angle in heterostructures of Ag nanoparticles randomly grown in Pt

Cite as: AIP Advances 9, 035025 (2019); doi: 10.1063/1.5079813
Presented: 15 January 2019 • Submitted: 3 November 2018 •
Accepted: 17 January 2019 • Published Online: 15 March 2019

O. Alves Santos,[1,2,a)] E. F. Silva,[1] M. Gamino,[1] J. B. S. Mendes,[2] S. M. Rezende,[1] and A. Azevedo[1]

AFFILIATIONS

[1] Departamento de Física, Universidade Federal de Pernambuco, 50670-901 Recife, Pernambuco, Brazil
[2] Departamento de Física, Universidade Federal de Viçosa, 36570-900 Viçosa, MG, Brazil

Note: This paper was presented at the 2019 Joint MMM-Intermag Conference.
[a)] **Corresponding author:** Obed Alves Santos, obed.alves@gmail.com

ABSTRACT

The spin Hall angle (SHA) represents the efficiency of the conversion between spin current into charge current and vice-versa. In this paper, we report the experimental detection of large enhancement of the effective SHA in heterostructures of yttrium iron garnet (YIG)/[Pt-Ag]/Pt and YIG/[Pt-Ag], when compared with measurements in YIG/Pt bilayers. The notation [Pt-Ag] represents the nanoparticles island formation of Ag in the Pt film. In order to investigate the role played by the metallic nanoparticles in the spin-to-charge conversion process, we carried out microwave spin pumping measurements in the following samples: YIG/Ag(3 nm)/Pt(6 nm), YIG/[Pt(3 nm)-Ag(3 nm)]/Pt(3 nm) and YIG/[Pt(6 nm)-Ag(3 nm)]. By means of high-resolution scanning electron microscope (HR-SEM) investigation, we confirmed that layers of Ag exhibit islands nanoparticle structures when grown on the surface of the Pt, which are characterized by the Volmer-Weber mode. The spin pumping results show that the Ag nanoparticles can enhance the charge current created by the inverse spin Hall effect (I_{ISHE}) up to three times larger than the single Pt layer. Also, by analyzing atomic force microscopy (AFM) images, obtained for samples with different thickness of the Ag layer, we conclude that the roughness plays an important role in the enhancement of the I_{ISHE}. Therefore, taking advantage of poor wetting properties of Ag over Pt layer, it was possible to create nanoscopic particles of Ag randomly grown in the Pt layer. The nanoparticles serve as nanoscopic molds to locally increase the SHA. This feature represents an improvement in searching more efficient methods of the spin-to-charge conversion and opens up the possibility of tuning the SHA by controlling the size and shape of the Ag nanoparticles.

The interplay between charge and spin transport is central to turn spintronics into a broad area of technological application based on the control and processing of the electron spin.[1,2] Two main topics in spintronics are the development of new spin-based devices and architectures as well as the search for more efficient methods and systems for spin-to-charge interconversion. One of the most common ways to convert charge current into spin current is the spin Hall effect (SHE),[3–6] where an unpolarized charge current in a metallic layer is partially converted in a transverse spin current by the spin-orbit coupling (SOC). The reciprocal of this effect is the inverse spin Hall effect (ISHE),[7,8] whereby a pure spin current is converted into a transverse charge current. In order to quantify the conversion efficiency between charge and spin currents in SHE and ISHE processes the spin Hall angle (θ_{SH}) is used, which is defined by the ratio between the spin Hall conductivity and the normal conductivity, i.e., $\theta_{SH} = \sigma^{s}_{yz}/\sigma^{c}_{xx}$.[3] The mechanisms behind the spin Hall angle (SHA), can be the intrinsic ones defined by the electronic structure of the crystalline material, or the extrinsic ones known as side jump and skew scattering,[9,10] where an electron is scattered off by impurities in combination with SOC. Once the control of intrinsic mechanisms to improve the SOC is not feasible, several theoretical and experimental schemes have been proposed in order to enhance the SOC extrinsically.[11–14] It is important to mention that among the pure elements, the high atomic number metals Pt, W, Pd and Ta, have

been regularly used for spin-charge interconversion because they have strong SOC, resulting in large θ_{SH}.[7,15–17]

In this paper we report the experimental studies using the spin pumping effect (SPE)[18] that detect an effective enhancement of the spin-to-charge conversion in Pt where nanoparticles of Ag were grown randomly, as shown in Figure 1 e). We have sputter deposited heterostructures of silver and platinum in three different arrangements as shown in Figures 1a) to c). The structures were grown by dc-sputtering on top of YIG ($Y_3Fe_5O_{12}$, Yttrium Iron Garnet) films with thickness of 100 nm and lateral dimensions of 3.5 mm × 1.7 mm.[19] As known, silver has poor wetting properties for surface coating.[20] Therefore, by taking advantage of this feature, we were able to grow nanoparticles of Ag on top of the Pt layer from the regime where the particles are isolated up to the regime where they collapse into a continuous film. By means of AFM images it was possible to conclude that the roughness plays an important role in the enhancement of the SHA.

The samples fabrication was accomplished in three steps: i) the YIG films were sputter deposited onto GGG(111) ($Gd_3Ga_5O_{12}$, Gadolinium Gallium Garnet) substrates. After deposition, the YIG layers were crystalized under oxygen flow for 4 hours at 850°; ii) then the YIG samples were characterized by means of the ferromagnetic resonance (FMR) technique in order to select the best samples and afterwards the layers of Ag and Pt were sputter grown; iii) Finally, two pads of Ag were deposited by means of shadow masks (1.7 mm × 400 μm × 20 nm) at the ends of the samples, where two electrodes of copper wires were attached with silver paste. All samples exhibited ohmic behavior as shown by their I-V characteristics. Figures 1 d) and e) show SEM images after deposition of an Ag layer with nominal thickness of 3 nm directly on YIG and on top of YIG/Pt(3 nm). The growth of Ag occurs by following the Volmer-Weber mode as shown in Figure 1 e).[21–23] This growth mode is characterized by the two-dimensional formation of 3D nanosized islands that further grow until reach the coalescence regime where it forms a continuous layer. Note that the sizes of Ag islands grown on top of the Pt layer are quite large. As discussed later, this characteristic is extremely important for the spin-charge enhancement.

In order to perform the FMR and SPE measurements, the samples were mounted on the tip of a polyvinyl chloride (PVC) rod and inserted through a hole in the back wall of a rectangular microwave cavity resonating at 9.46 GHz, operating in the TE_{102} mode, with a Q factor of 2000 and an incident rf power P_{rf} = 20 mW. Figure 2 a) shows the field scan of the derivative dP/dH of the microwave absorption at the FMR condition (black symbols) for YIG/Pt sample. By numerically adjusting the data with the derivative of a Lorentzian function (solid red line) we obtain the FMR field and the linewidth. The inset shows the FMR from bare YIG with no metal layer deposition. All bare YIG films have FMR linewidths that vary from 7.4 to 8.4 Oe. In average, the FMR linewidths experienced an additional increase of 1.2 Oe after the metal layer deposition, which is a signature of the SPE.[18] Figure 2 b) shows schematically the SPE and the spin-to-charge conversion process by ISHE. The pure spin current injected at the YIG/Pt interface is be given by $\vec{J}_S = \left(\hbar g_{eff}^{\uparrow\downarrow}/4\pi\right)\left(\hat{m} \times \frac{d\hat{m}}{dt}\right)$, where $\hat{m}$ is a unit vector along the magnetization direction and $g_{eff}^{\uparrow\downarrow} = (4\pi M_S t_{FM}/\hbar\omega)\delta H$ is the real part of the effective spin-mixing conductance that takes into account the pumped and the back-flow spin currents.[18] In this equation the additional FMR linewidth $\delta H = (\Delta H_{YIG/Pt-Ag} - \Delta H_{YIG})$ is assumed to be entirely due to the spin pumping effect, ω is the microwave frequency, t_{FM} and $4\pi M_S$ = 1760 G are, respectively, the thickness and saturation magnetization of YIG layer. The relation between charge current and spin current in the ISHE process is given by $\vec{J}_C = \theta_{SH}(2e/\hbar)\left(\vec{\sigma} \times \vec{J}_S\right)$, where θ_{SH} is the spin Hall angle, and $\vec{\sigma}$ is the dc component of spin-current polarization, which is parallel to dc magnetic field. Integrating the charge current along the sample thickness and length, one can write the spin pumping voltage between the edges of NM as,[24–26]

$$V_{\mathrm{ISHE}} = R_N w \lambda_N \left(\frac{2e}{\hbar}\right)\theta_{SH} \tanh\left(\frac{t_N}{2\lambda_N}\right) J_{Sy}(0) \cos\alpha, \qquad (1)$$

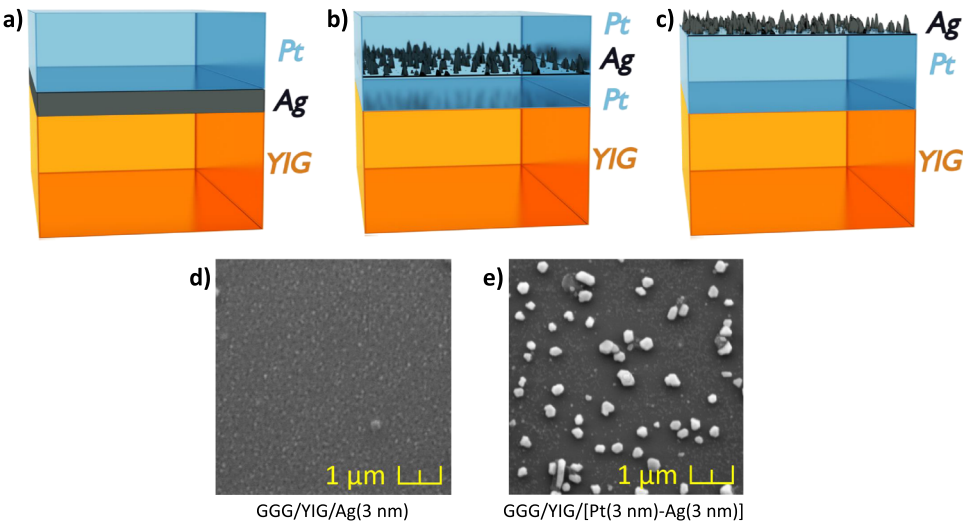

FIG. 1. Sketch of the three grown heterostructures, a) YIG/Ag(3 nm)/Pt(6 nm), b) YIG/[Pt(3 nm)-Ag(3 nm)]/Pt(3 nm) and c) YIG/[Pt(6 nm)-Ag(3 nm)]. The notation [Pt-Ag] represents the nanoparticles island formation of Ag on the Pt film and the nominal thickness in nm. The SEM microscopy image, shown in d), confirms that Ag nicely wets the YIG surface. On the other hand, when deposited on top of Pt, Ag grows by means of islands, as shown in e).

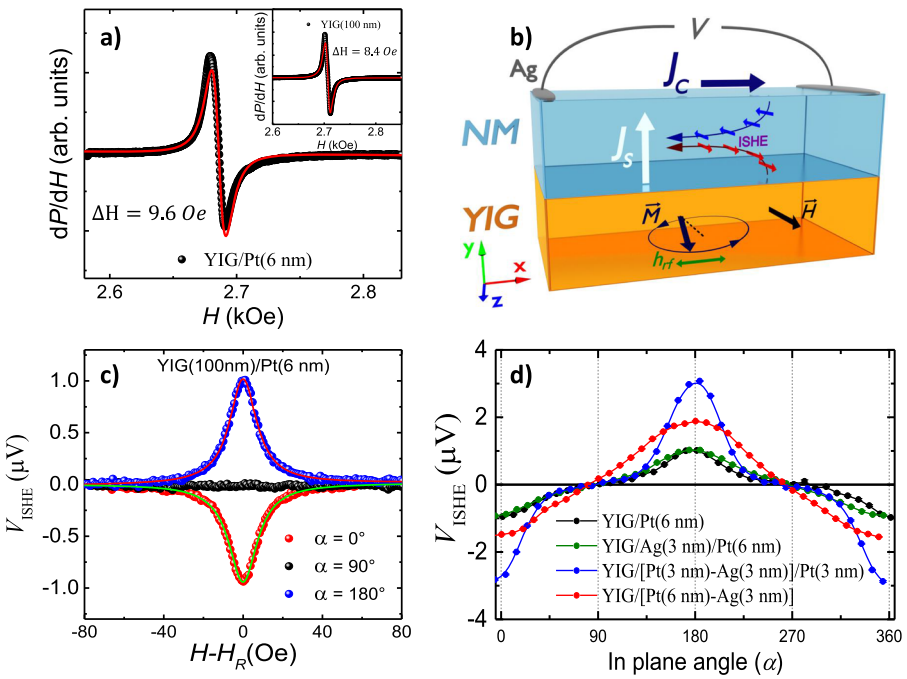

FIG. 2. a) Field scan of the derivative of the FMR absorption of YIG/Pt. The inset show the FMR of bare YIG before the metal layer deposition. b) Illustration of spin pumping process and conversion of spin current into charge current by ISHE. c) V_{ISHE} for three field angles in the plane of the sample, the red and green solid lines correspond to best fit to the data with equation (2). d) Angular dependence of the symmetric component of V_{ISHE} for different samples.

where R_N, λ_N, w, t_N are, respectively, the resistance, spin diffusion length, width and thickness of conductive layer, $J_{Sy}(0)$ is the spin current density at the interface YIG/NM, and α is the in-plane angle between magnetic field and the direction of the electric contacts at the ends of sample.

Figure 2 c) shows the field-scan dependence of spin pumping voltage (V_{ISHE}) of YIG/Pt for three key alpha angles. The measured line shapes of V_{ISHE} are normally asymmetric curves, which are fitted as a sum of a Lorentzian function and its derivative, centered at the FMR field,

$$V_{\mathrm{ISHE}} = V_s \frac{\Delta H^2}{\left[(H-H_R)^2 - \Delta H^2\right]} + V_a \frac{\left[-2\Delta H(H-H_R)\right]}{\left[(H-H_R)^2 - \Delta H^2\right]}, \quad (2)$$

where H_R and ΔH are, the FMR field and linewidth (HWHM). The red and green lines of Figure 2 c) correspond to the best fit to the data with equation (2), where V_s, (V_a) denote the amplitude of symmetric, (antisymmetric) components. The voltage V_s is attributed to ISHE voltage in Eq (1), while the antisymmetric amplitude depends on the anisotropic magnetoresistance component.[24] Figure 2 d) shows the angular dependence of the V_s for the entire series of samples investigated here. The maximum V_{ISHE} measured for a single Pt layer was $V_{\mathrm{ISHE}}^{Pt} = 1\,\mu V$, as shown by the black symbols in Fig. 2d). When the Ag nanoparticles are directly deposited on the YIG surface and then covered by Pt, as in YIG/Ag(3 nm)/Pt(6 nm), the measured voltage was also $V_{\mathrm{ISHE}}^{Ag/Pt} \approx 1\,\mu V$, as seen by the green symbols of Fig. 2d). However, when the Ag islands are grown in the midst of the Pt layer, as in YIG/[Pt(3 nm)-Ag(3 nm)]/Pt(3 nm), V_{ISHE} reaches a value 3 times larger, i.e., $V_{\mathrm{ISHE}}^{Pt/Ag/Pt} \approx 3\,\mu V$, (see the blue symbols of Fig. 2d)). When the Ag islands are grown on the top surface of the Pt layer, as in YIG/[Pt(6 nm)-Ag(3 nm)], V_{ISHE} decreases a little, $V_{\mathrm{ISHE}}^{Pt/Ag} \approx 2\,\mu V$ (red symbols in Fig. 2d)). While the V_a component is negligible in all cases, as expected for a FM insulator, the in-plane dependence of V_s departs a little from the expected cos α in Figures 2 d). As V_{ISHE} depends on the resistance of the NM layer, the SPE-ISHE current, written as ($I_{\mathrm{ISHE}} = V_{\mathrm{ISHE}}/R_N$), has more physical meaning. The parameters ΔH, δH, $g_{eff}^{\uparrow\downarrow}$, R_N and I_{ISHE} for all samples is shown on Table I.

In Eq. (1), the dc component of the spin current at the interface YIG/NM is given by $J_{Sy}(0) = \frac{\hbar\omega p g_{eff}^{\uparrow\downarrow}}{16\pi}\left(\frac{h_{rf}}{\Delta H}\right)^2 L(H-H_R)$, where

TABLE I. Linewidth, additional FMR linewidth, spin mixing conductance, resistance and I_{ISHE} for all the samples.

Sample	ΔH (Oe)	δH (Oe)	$g_{eff}^{\uparrow\downarrow}$ (m^{-2})	R_N (Ω)	I_{ISHE} (nA)
YIG/Pt(6 nm)	9.6	1.24	3.37×10^{18}	92	11.0
YIG/Ag(3 nm)/Pt(6 nm)	9.2	1.12	3.37×10^{18}	78	13.2
YIG/[Pt(3 nm)-Ag(3 nm)]/Pt(3 nm)	8.9	1.06	3.09×10^{18}	80	37.0
YIG/[Pt(6 nm)-Ag(3 nm)]	8.5	1.21	3.41×10^{18}	65	31.3

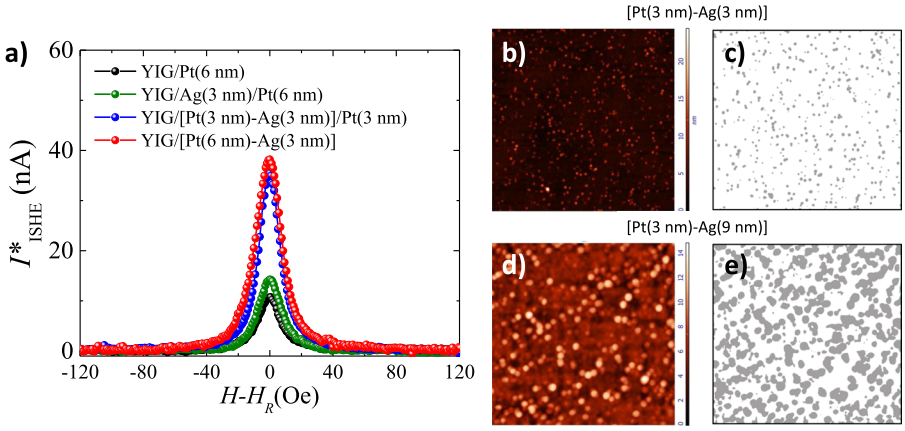

FIG. 3. a) Field scan of I^*_{ISHE} for different samples where the Ag particles are grown in different positions of the stack. On the right is shown AFM images b) and d) and flooded images c) and e) respectively for samples [Pt(3 nm)-Ag(3 nm)] and [Pt(3 nm)-Ag(9 nm)]. To calculate the average nanoparticle size, the same height threshold was used in the flooded images analysis. The surface area of the images are 2.0 μm × 2.0 μm.

$L(H - H_R) = 1$ at the ferromagnetic resonance condition and p is the precession ellipticity. Since V_{ISHE} and $I_{ISHE}(=V_{ISHE}/R)$ are proportional to $(1/\Delta H)^2$, we need to take into account a contribution from fluctuation effects of the FMR linewidth to the maximum values of both V_{ISHE} and I_{ISHE}. Therefore, we define the maximum value of spin pumping current as $I^*_{ISHE} = I_{ISHE}(\Delta H/\Delta H_{Pt})^2$, where ΔH is the linewidth of the sample with Ag nanoparticles and ΔH_{Pt} is the linewidth of the sample with no Ag particles (YIG/Pt (6 nm)). Figure 3 a) shows the field dependence of I^*_{ISHE} after the renormalization procedure. As the maximum value of I^*_{ISHE} can be written as $I^{*peak}_{ISHE} = w\lambda_N \omega p g^{\uparrow\downarrow}_{eff}\theta_{SH}$, and the parameters w, ω, p and $g^{\uparrow\downarrow}_{eff}$ are the same for all samples and $\lambda_N = \lambda_{Pt}$, we conclude that $I^{*peak}_{ISHE} \propto \theta_{SH}$. The result shown in Figure 3 a) confirms that the nanoparticles of Ag in the Pt layer are playing a key role in the enhancement of the effective spin Hall angle θ_{SH}. The enhancement of θ_{SH} is the same, for the samples with Ag nanoparticles placed above the Pt layer YIG/[Pt(6 nm)/Ag(3 nm)] (red symbols) and in the middle of the Pt layer YIG/[Pt(3 nm)-Ag(3 nm)]/Pt(3 nm) (blue symbols). The sample YIG/Ag(3 nm)/Pt(6 nm) did not show significative increase of I_{ISHE} due to the fact that when Ag is deposited directly on top of YIG (green symbols) it creates an more uniform layer of Ag.

We also investigate the surface topography by means of the atomic force microscopy (AFM) technique and we were able to measure the average size of the nanoparticles as a function of the nominal Ag layer thickness. Figures 3 b) and d) shows the topography of b) [Pt(3 nm)-Ag(3 nm)] and d) [Pt(3 nm)-Ag(9 nm)] measured in an area of (2.0 μm × 2.0 μm). By using the flooding tool of the software "Image Analysis", it was possible to investigate the images as a function of the height threshold. In Figs. 3 c) and e) it is shown the nanoparticles with average size of Ag nanoparticles of 39 nm, for the sample [Pt(3 nm)-Ag(3 nm)], and 59 nm, for the sample [Pt(3 nm)-Ag(9 nm)]. Clearly the sample [Pt(3 nm)-Ag(9 nm)] exhibits a surface with large number of clusters close to the coalescence threshold. Evaluating the average roughness (δ) of the samples we obtain an increasing from $\delta^{Ag}_{3\,nm} = 0.95$ nm to $\delta^{Ag}_{9\,nm} = 1.65$ nm, then a decreasing to $\delta^{Ag}_{15\,nm} = 0.95$ nm. This result confirms that the sample with $t_{Ag} = 9\ nm$ is rougher and is in the threshold to turns into a continuous Ag layer. As shown in Ref. 19, the samples with $t_{Ag} > 9\ nm$ exhibit a decrease of the effective spin Hall angle, which validates the assumption that Ag nanoparticles are playing a key role in the enhancement of the spin to charge conversion process. Our results support the theoretical prediction of Ref. 12 that proposes an enhancement of the spin Hall angle as a function of the roughness δ.

In summary, we conclude that taking advantage the pour wetting proprieties of Ag over Pt layer, it was possible to create nanoscopic particles of Ag on top and on the middle plane of Pt layer. Those nanoparticles serve as nanoscopic molds to locally increase the spin Hall angle, thus effectively increasing the efficiency of spin current to charge current. These results represent a reliable technique to locally control the effective spin Hall angle in order to reach higher values of SHA. The extrinsic enhancement of θ_{SH}, by the nanoscopic particles of Ag and Cu, was also confirmed by others spin-charge interconversion techniques, such as spin Seebeck effect and spin Hall magnetoresistance.[19,27]

This research was supported by the Brazilian agencies Conselho Nacional de Desenvolvimento Científico e Tecnológico (CNPq), Coordenação de Aperfeiçoamento de Pessoal de Nível Superior (CAPES), Financiadora de Estudos e Projetos (FINEP), Fundação de Amparo à Ciência e Tecnologia de Pernambuco (FACEPE), Fundação de Amparo à Pesquisa do Estado de Minas Gerais (FAPEMIG).

REFERENCES

[1] S. A. Wolf *et al.*, "Spintronics: A spin-based electronics vision for the future," Science **294**, 1488–1495 (2001).
[2] I. Žutić, J. Fabian, and S. D. Sarma, "Spintronics: Fundamentals and applications," Reviews of Modern Physics **76**, 323–410 (2004).
[3] J. E. Hirsch, "Spin Hall effect," Phys. Rev. Lett. **83**, 1834–1837 (1999).
[4] M. I. D'yakonov and V. I. Perel', "Possibility of orienting electron spins with current," JETP Lett. **13**, 467–469 (1971).
[5] Y. K. Kato, R. C. Myers, A. C. Gossard, and D. D. Awschalom, "Observation of the spin Hall effect in semiconductors," Science **306**, 1910–1913 (2004).
[6] J. Wunderlich, B. Kaestner, J. Sinova, and T. Jungwirth, "Experimental observation of the spin-Hall effect in a two-dimensional spin-orbit coupled semiconductor system," Phys. Rev. Lett. **94**, 047204 (2005).

[7]A. Azevedo, L. H. Vilela Leão, R. L. Rodriguez-Suarez, A. B. Oliveira, and S. M. Rezende, "dc effect in ferromagnetic resonance: Evidence of the spin-pumping effect?," J. Appl. Phys. **97**, 10C715 (2005).
[8]E. Saitoh, M. Ueda, H. Miyajima, and G. Tatara, "Conversion of spin current into charge current at room temperature: Inverse spin-Hall effect," Appl. Phys. Lett. **88**, 182509 (2006).
[9]L. Berger, "Side-jump mechanism for the Hall effect of ferromagnets," Phys. Rev. B **2**, 4559–4566 (1970).
[10]J. Smit, "The spontaneous Hall effect in ferromagnetics II," Physica **24**, 39–51 (1958).
[11]Y. Niimi and Y. Otani, "Reciprocal spin Hall effects in conductors with strong spin–orbit coupling: A review," Reports Prog. Phys. **78**, 124501 (2015).
[12]L. Zhou, V. L. Grigoryan, S. Maekawa, X. Wang, and J. Xiao, "Spin Hall effect by surface roughness," Phys. Rev. B **91**, 045407 (2015).
[13]L. Wang *et al.*, "Giant room temperature interface spin Hall and inverse spin Hall effects," Phys. Rev. Lett. **116**, 196602 (2016).
[14]M. Obstbaum *et al.*, "Tuning spin Hall angles by alloying," Phys. Rev. Lett. **117**, 167204 (2016).
[15]L. Liu *et al.*, "Spin-torque switching with the giant spin Hall effect of tantalum," Science **336**, 555–558 (2012).
[16]C.-F. Pai *et al.*, "Spin transfer torque devices utilizing the giant spin Hall effect of tungsten," Appl. Phys. Lett. **101**, 122404 (2012).
[17]H. L. Wang *et al.*, "Scaling of spin Hall angle in 3d, 4d, and 5d metals from $Y_3Fe_5O_{12}$/metal spin pumping," Phys. Rev. Lett. **112**, 197201 (2014).
[18]Y. Tserkovnyak, A. Brataas, and G. E. W. Bauer, "Enhanced Gilbert damping in thin ferromagnetic films," Phys. Rev. Lett. **88**, 117601 (2002).
[19]O. Alves-Santos *et al.*, "Giant spin-charge conversion driven by nanoscopic particles of Ag in Pt," Phys. Rev. B **96**, 060408 (2017).
[20]J. A. Venables, G. D. T. Spiller, and M. Hanbucken, "Nucleation and growth of thin films," Reports Prog. Phys. **47**, 399–459 (1984).
[21]G. Abadias *et al.*, "Volmer-Weber growth stages of polycrystalline metal films probed by *in situ* and real-time optical diagnostics," Appl. Phys. Lett. **107**, 183105 (2015).
[22]J. C. Glueckstein, M. M. R. Evans, and J. Nogami, "Surface unwetting during growth of Ag on Si(001)," Phys. Rev. B **54**, R11066–R11069 (1996).
[23]P. W. Davies, M. A. Quinlan, and G. A. Somorjai, "The growth and chemisorptive propertles of Ag and Au monolayers on platinum single crystal surfaces: An AES, TDS and LEED study," Surf. Sci. **121**, 290–302 (1982).
[24]A. Azevedo, L. H. Vilela-Leão, R. L. Rodríguez-Suárez, A. F. Lacerda Santos, and S. M. Rezende, "Spin pumping and anisotropic magnetoresistance voltages in magnetic bilayers: Theory and experiment," Phys. Rev. B **83**, 144402 (2011).
[25]O. Mosendz *et al.*, "Quantifying spin Hall angles from spin pumping: Experiments and theory," Phys. Rev. Lett. **104**, 046601 (2010).
[26]A. Hoffmann, "Spin Hall effects in metals," IEEE Trans. Magn. **49**, 5172–5193 (2013).
[27]M. Gamino *et al.*, "The role of metallic nanoparticles in the enhancement of the spin Hall magnetoresistance in YIG/Pt thin films," J. Magn. Magn. Mater. **466**, 267–272 (2018).